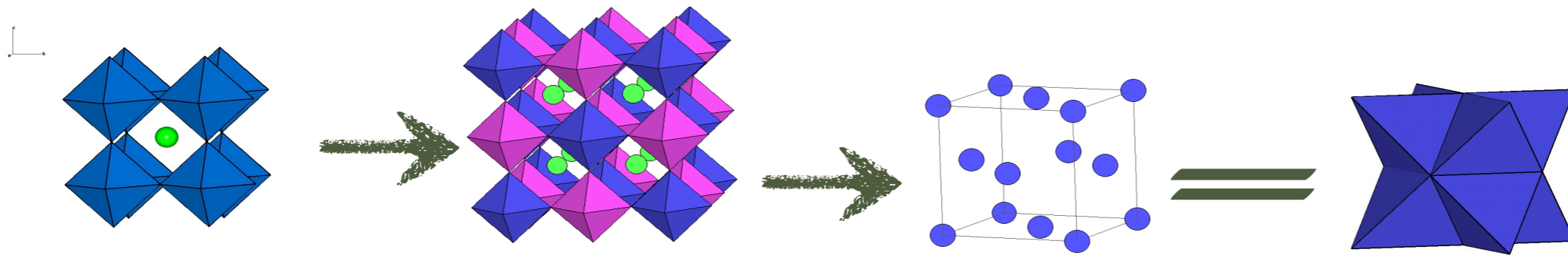


Ba_2YMoO_6 : a “QSL” with
(strong) spin-orbit coupling?

Gang Chen
University of Colorado, Boulder

ORDERED DOUBLE PEROVSKITES

FCC ordered double perovskites $A_2BB'O_6$



| Compound | B' config. | crystal structure | θ_{CW} | $\mu_{eff}(\mu_B)$ | magnetic transition | frustration parameter f |
|---------------|-----------------|---|---------------|--------------------|----------------------------|---------------------------|
| Ba_2YMoO_6 | $Mo^{5+}(4d^1)$ | cubic | -91K | 1.34 | PM down to 2K | $f \gtrsim 45$ |
| Ba_2YMoO_6 | $Mo^{5+}(4d^1)$ | cubic | -160K | 1.40 | PM down to 2K | $f \gtrsim 80$ |
| Ba_2YMoO_6 | $Mo^{5+}(4d^1)$ | cubic | -219K | 1.72 | PM down to 2K | $f \gtrsim 100$ |
| La_2LiMoO_6 | $Mo^{5+}(4d^1)$ | monoclinic | -45K | 1.42 | PM to 2K | $f \gtrsim 20$ |
| Sr_2MgReO_6 | $Re^{6+}(5d^1)$ | tetragonal | -426K | 1.72 | spin glass, $T_G \sim 50K$ | $f \gtrsim 8$ |
| Sr_2CaReO_6 | $Re^{6+}(5d^1)$ | monoclinic | -443K | 1.659 | spin glass, $T_G \sim 14K$ | $f \gtrsim 30$ |
| Ba_2CaReO_6 | $Re^{6+}(5d^1)$ | cubic to tetragonal (at $T \sim 120K$) | -38.8K | 0.744 | AFM $T_c = 15.4K$ | $f \sim 2$ |
| Ba_2LiOsO_6 | $Os^{7+}(5d^1)$ | cubic | -40.48K | 0.733 | AFM $T_c \sim 8K$ | $f \gtrsim 5$ |
| Ba_2NaOsO_6 | $Os^{7+}(5d^1)$ | cubic | -32.45K | 0.677 | FM $T_c \sim 8K$ | $f \gtrsim 4$ |
| Ba_2NaOsO_6 | $Os^{7+}(5d^1)$ | cubic | $\sim -10K$ | ~ 0.6 | FM $T_c = 6.8K$ | $f \gtrsim 4$ |

There also exist d^2 and d^3 double perovskites

M.A. de Vries et al, PRL 2010, T. Aharen et al PRB 2010

J.P. Carlo et al, PRB 2011

K. E. Stitzer, et al, Solid State Sciences 4, 2002 (311)

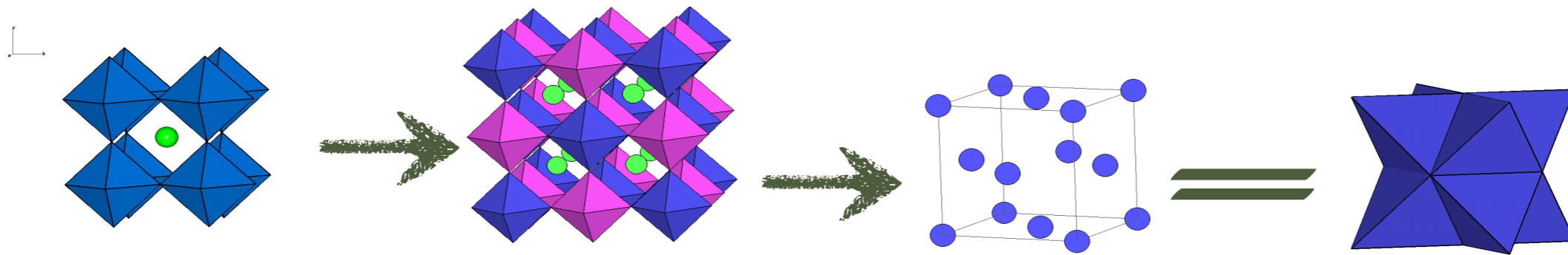
A.S.Erickson, et al PRL 2007

C. Wiebe, et al PRB 2002, 2003

K. Yamamura, et al, Journal Solid State Chemistry 179, 605 (2006).

ORDERED DOUBLE PEROVSKITES

FCC ordered double perovskites $A_2BB'O_6$



| Compound | B' config. | crystal structure | θ_{CW} | $U_{eff}(U_B)$ | magnetic transition | frustration parameter f |
|------------------------------------|-------------------------------------|---|---------------|----------------|----------------------------|---------------------------|
| Ba ₂ YMoO ₆ | Mo ⁵⁺ (4d ¹) | cubic | -91K | 1.34 | PM down to 2K | $f \gtrsim 45$ |
| Ba ₂ YMoO ₆ | Mo ⁵⁺ (4d ¹) | cubic | -160K | 1.40 | PM down to 2K | $f \gtrsim 80$ |
| Ba ₂ YMoO ₆ | Mo ⁵⁺ (4d ¹) | cubic | -219K | 1.72 | PM down to 2K | $f \gtrsim 100$ |
| La ₂ LiMoO ₆ | Mo ³⁺ (4d ¹) | monoclinic | -45K | 1.42 | PM to 2K | $f \gtrsim 20$ |
| Sr ₂ MgReO ₆ | Re ⁶⁺ (5d ¹) | tetragonal | -426K | 1.72 | spin glass, $T_G \sim 50K$ | $f \gtrsim 8$ |
| Sr ₂ CaReO ₆ | Re ⁶⁺ (5d ¹) | monoclinic | -443K | 1.659 | spin glass, $T_G \sim 14K$ | $f \gtrsim 30$ |
| Ba ₂ CaReO ₆ | Re ⁶⁺ (5d ¹) | cubic to tetragonal (at $T \sim 120K$) | -38.8K | 0.744 | AFM $T_c = 15.4K$ | $f \sim 2$ |
| Ba ₂ LiOsO ₆ | Os ⁷⁺ (5d ¹) | cubic | -40.48K | 0.733 | AFM $T_c \sim 8K$ | $f \gtrsim 5$ |
| Ba ₂ NaOsO ₆ | Os ⁷⁺ (5d ¹) | cubic | -32.45K | 0.677 | FM $T_c \sim 8K$ | $f \gtrsim 4$ |
| Ba ₂ NaOsO ₆ | Os ⁷⁺ (5d ¹) | cubic | $\sim -10K$ | ~ 0.6 | FM $T_c = 6.8K$ | $f \gtrsim 4$ |

Likely to be
a QSL

There also exist d^2 and d^3 double perovskites

M.A. de Vries et al, PRL 2010, T. Aharen et al PRB 2010

J.P. Carlo et al, PRB 2011

K. E. Stitzer, et al, Solid State Sciences 4, 2002 (311)

A.S.Erickson, et al PRL 2007

C. Wiebe, et al PRB 2002, 2003

K. Yamamura, et al, Journal Solid State Chemistry 179, 605 (2006).

Valence Bond Glass on an fcc Lattice in the Double Perovskite Ba_2YMoO_6

M. A. de Vries,^{1,2,*} A. C. Mclaughlin,³ and J.-W. G. Bos^{4,5}

¹*School of Physics and Astronomy, E. C. Stoner Laboratory, University of Leeds, Leeds, LS2 9JT, United Kingdom*

²*School of Physics & Astronomy, University of St-Andrews, the North Haugh, KY16 9SS, United Kingdom*

³*Department of Chemistry, University of Aberdeen, Meston Walk, Aberdeen AB24 3UE, United Kingdom*

⁴*School of Chemistry, University of Edinburgh, King's Buildings, Mayfield Road, Edinburgh EH9 3JZ, United Kingdom*

⁵*Department of Chemistry - EPS, Heriot-Watt University, Edinburgh, EH14 4AS, United Kingdom*

(Received 10 November 2009; revised manuscript received 6 April 2010; published 27 April 2010)

We report on the unconventional magnetism in the cubic *B*-site ordered double perovskite Ba_2YMoO_6 , using ac and dc magnetic susceptibility, heat capacity and muon spin rotation. No magnetic order is observed down to 2 K while the Weiss temperature is ~ -160 K. This is ascribed to the geometric frustration in the lattice of edge-sharing tetrahedra with orbitally degenerate Mo^{5+} $s = 1/2$ spins. Our experimental results point to a gradual freezing of the spins into a disordered pattern of spin singlets, quenching the orbital degeneracy while leaving the global cubic symmetry unaffected, and providing a rare example of a valence bond glass.

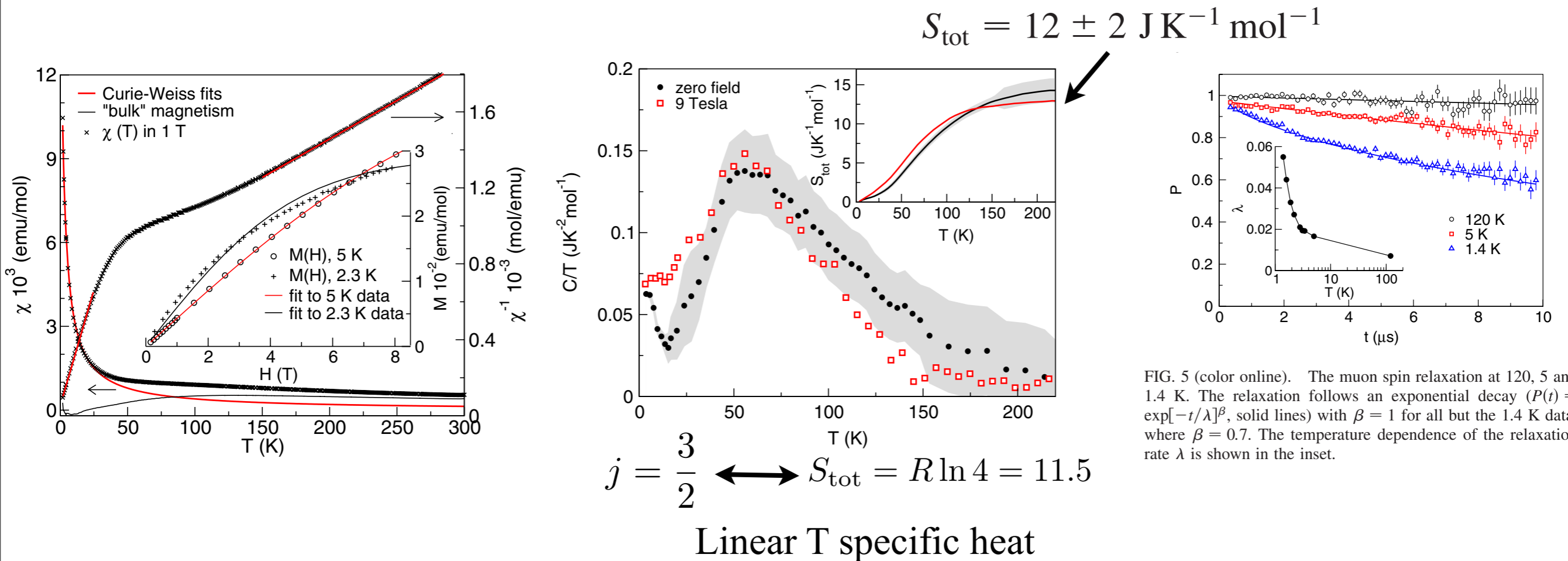


FIG. 5 (color online). The muon spin relaxation at 120, 5 and 1.4 K. The relaxation follows an exponential decay ($P(t) = \exp[-t/\lambda]^\beta$, solid lines) with $\beta = 1$ for all but the 1.4 K data, where $\beta = 0.7$. The temperature dependence of the relaxation rate λ is shown in the inset.

Magnetic properties of the geometrically frustrated $S = \frac{1}{2}$ antiferromagnets, $\text{La}_2\text{LiMoO}_6$ and Ba_2YMoO_6 , with the B-site ordered double perovskite structure: Evidence for a collective spin-singlet ground state

Tomoko Aharen,¹ John E. Greedan,^{1,2} Craig A. Bridges,¹ Adam A. Aczel,³ Jose Rodriguez,³ Greg MacDougall,³ Graeme M. Luke,^{2,3,4} Takashi Imai,^{2,3,4} Vladimir K. Michaelis,⁵ Scott Kroecker,⁵ Haidong Zhou,⁶ Chris R. Wiebe,^{6,7} and Lachlan M. D. Cranswick⁸

¹Department of Chemistry, McMaster University, Hamilton, Ontario, Canada L8S 4M1

²Brockhouse Institute of Material Research, McMaster University, Hamilton, Ontario, Canada L8S 4M1

³Department of Physics and Astronomy, McMaster University, Hamilton, Ontario, Canada L8S 4M1

⁴Canadian Institute for Advanced Research, Toronto, Ontario, Canada M5G 1Z8

⁵Department of Chemistry, University of Manitoba, Winnipeg, Manitoba, Canada R3T 2N2

⁶Department of Physics, Florida State University, Tallahassee, Florida 32310-4005, USA

⁷Department of Chemistry, University of Winnipeg, Winnipeg, Manitoba, Canada R3B 2E9

⁸Canadian Neutron Beam Centre, National Research Council, Chalk River Laboratories, Chalk River, Ontario, Canada K0J 1J0

(Received 4 January 2010; revised manuscript received 21 April 2010; published 4 June 2010)

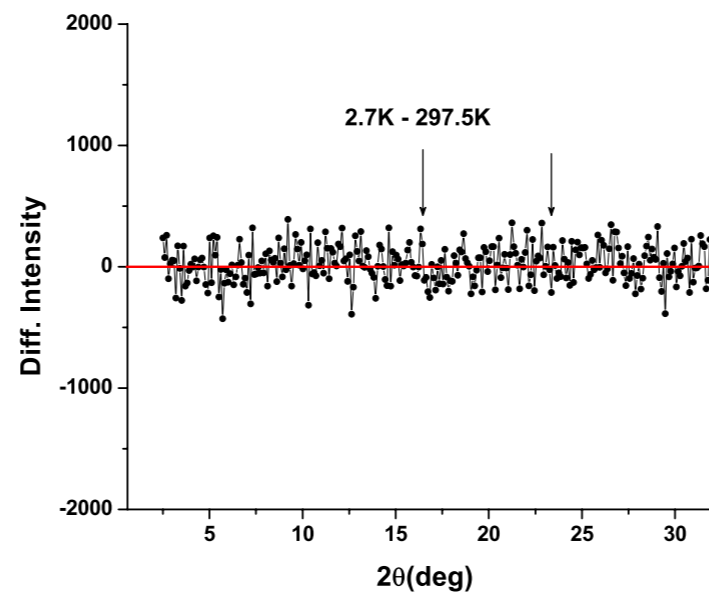
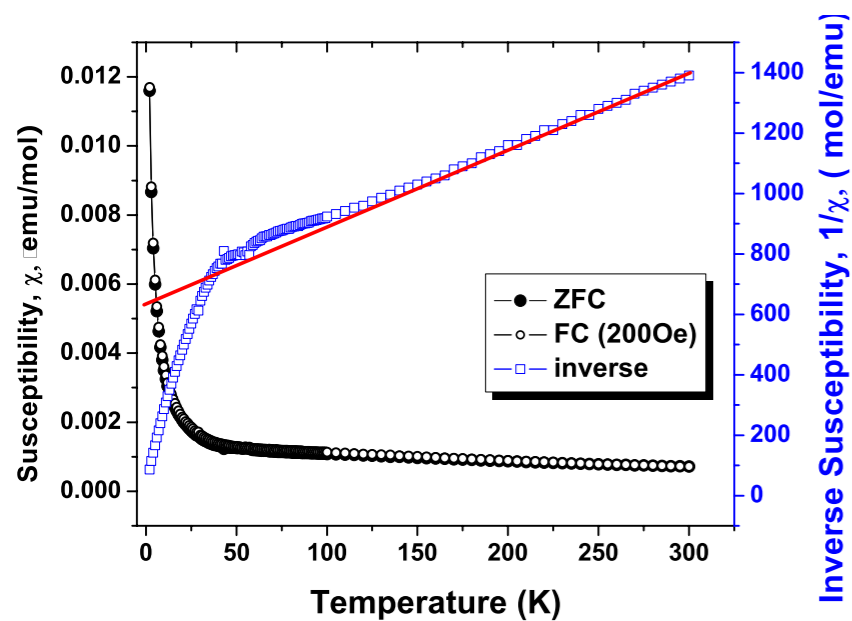
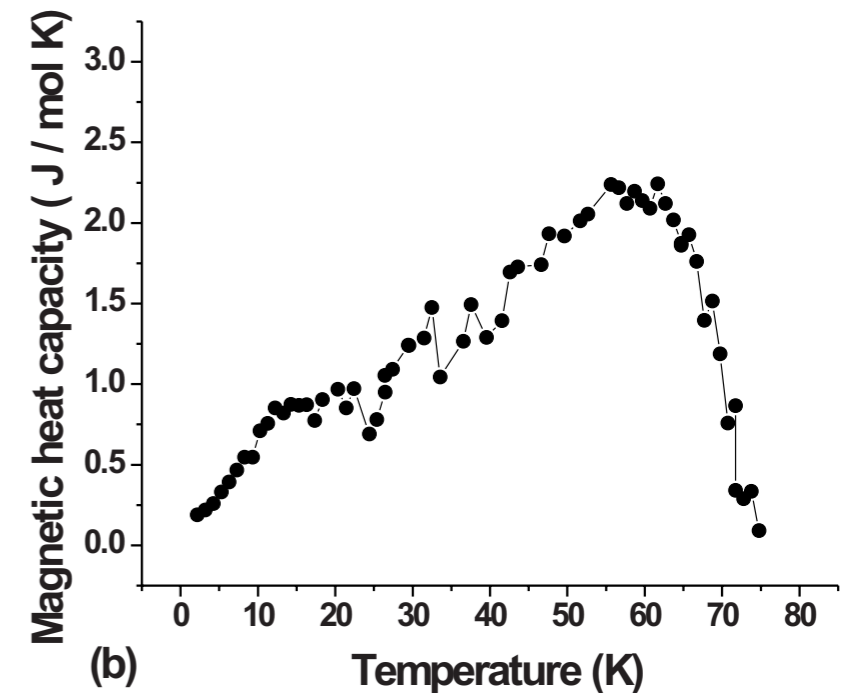


FIG. 11. (Color online) Neutron-diffraction difference pattern, 2.7–297.5 K for Ba_2YMoO_6 . The arrows show the expected positions of magnetic reflections assuming a type 1 fcc magnetic structure as found for Ba_2YRuO_6 (Ref. 6).



Magnetic properties of the geometrically frustrated $S = \frac{1}{2}$ antiferromagnets, $\text{La}_2\text{LiMoO}_6$ and Ba_2YMoO_6 , with the B-site ordered double perovskite structure: Evidence for a collective spin-singlet ground state

Tomoko Aharen,¹ John E. Greedan,^{1,2} Craig A. Bridges,¹ Adam A. Aczel,³ Jose Rodriguez,³ Greg MacDougall,³ Graeme M. Luke,^{2,3,4} Takashi Imai,^{2,3,4} Vladimir K. Michaelis,⁵ Scott Kroecker,⁵ Haidong Zhou,⁶ Chris R. Wiebe,^{6,7} and Lachlan M. D. Cranswick⁸

¹Department of Chemistry, McMaster University, Hamilton, Ontario, Canada L8S 4M1

²Brockhouse Institute of Material Research, McMaster University, Hamilton, Ontario, Canada L8S 4M1

³Department of Physics and Astronomy, McMaster University, Hamilton, Ontario, Canada L8S 4M1

⁴Canadian Institute for Advanced Research, Toronto, Ontario, Canada M5G 1Z8

⁵Department of Chemistry, University of Manitoba, Winnipeg, Manitoba, Canada R3T 2N2

⁶Department of Physics, Florida State University, Tallahassee, Florida 32310-4005, USA

⁷Department of Chemistry, University of Winnipeg, Winnipeg, Manitoba, Canada R3B 2E9

⁸Canadian Neutron Beam Centre, National Research Council, Chalk River Laboratories, Chalk River, Ontario, Canada K0J 1J0

(Received 4 January 2010; revised manuscript received 21 April 2010; published 4 June 2010)

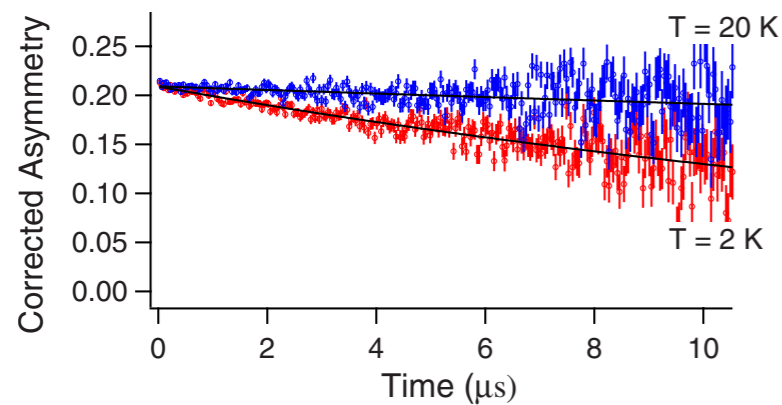


FIG. 13. (Color online) ZF μSR data for Ba_2YMoO_6 for two temperatures. The lines are fits to a single exponential relaxation function, see text.

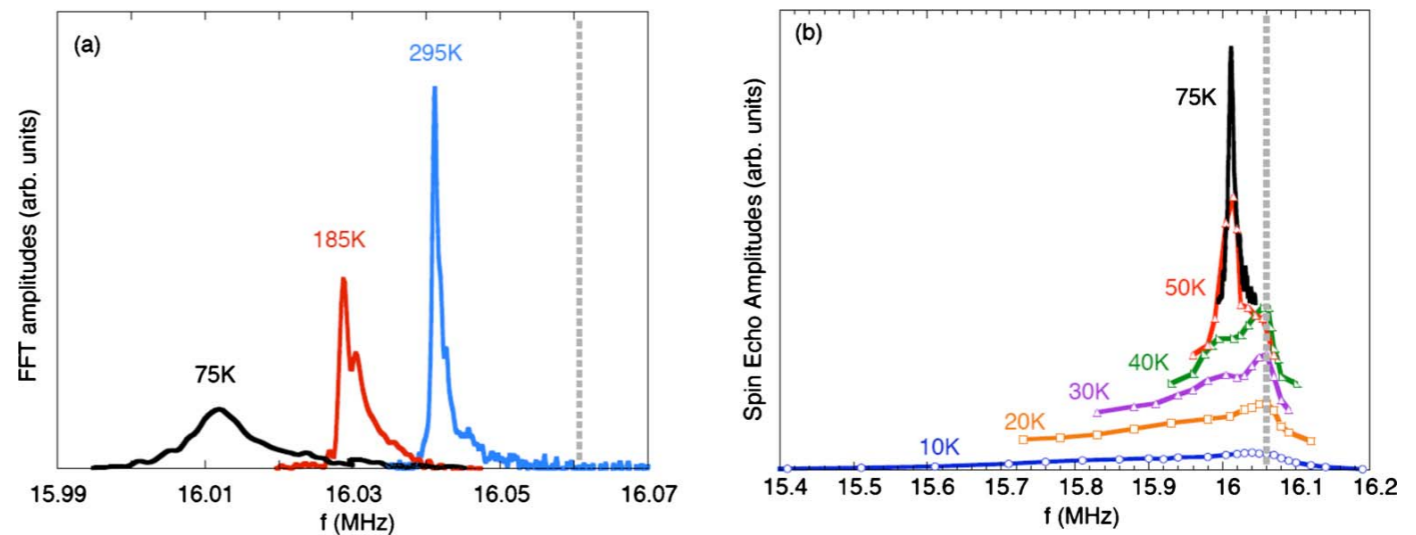


FIG. 14. (Color online) ^{89}Y NMR line shape at various temperatures. (a) Representative line shapes at selected temperatures for Ba_2YMoO_6 . (b) Evolution of the line shape below 75 K.

Magnetic properties of the geometrically frustrated $S = \frac{1}{2}$ antiferromagnets, $\text{La}_2\text{LiMoO}_6$ and Ba_2YMoO_6 , with the B-site ordered double perovskite structure: Evidence for a collective spin-singlet ground state

Tomoko Aharen,¹ John E. Greedan,^{1,2} Craig A. Bridges,¹ Adam A. Aczel,³ Jose Rodriguez,³ Greg MacDougall,³
Graeme M. Luke,^{2,3,4} Takashi Imai,^{2,3,4} Vladimir K. Michaelis,⁵ Scott Kroeker,⁵ Haidong Zhou,⁶
Chris R. Wiebe,^{6,7} and Lachlan M. D. Cranswick⁸

¹*Department of Chemistry, McMaster University, Hamilton, Ontario, Canada L8S 4M1*

²*Brockhouse Institute of Material Research, McMaster University, Hamilton, Ontario, Canada L8S 4M1*

³*Department of Physics and Astronomy, McMaster University, Hamilton, Ontario, Canada L8S 4M1*

⁴*Canadian Institute for Advanced Research, Toronto, Ontario, Canada M5G 1Z8*

⁵*Department of Chemistry, University of Manitoba, Winnipeg, Manitoba, Canada R3T 2N2*

⁶*Department of Physics, Florida State University, Tallahassee, Florida 32310-4005, USA*

⁷*Department of Chemistry, University of Winnipeg, Winnipeg, Manitoba, Canada R3B 2E9*

⁸*Canadian Neutron Beam Centre, National Research Council, Chalk River Laboratories, Chalk River, Ontario, Canada K0J 1J0*

(Received 4 January 2010; revised manuscript received 21 April 2010; published 4 June 2010)

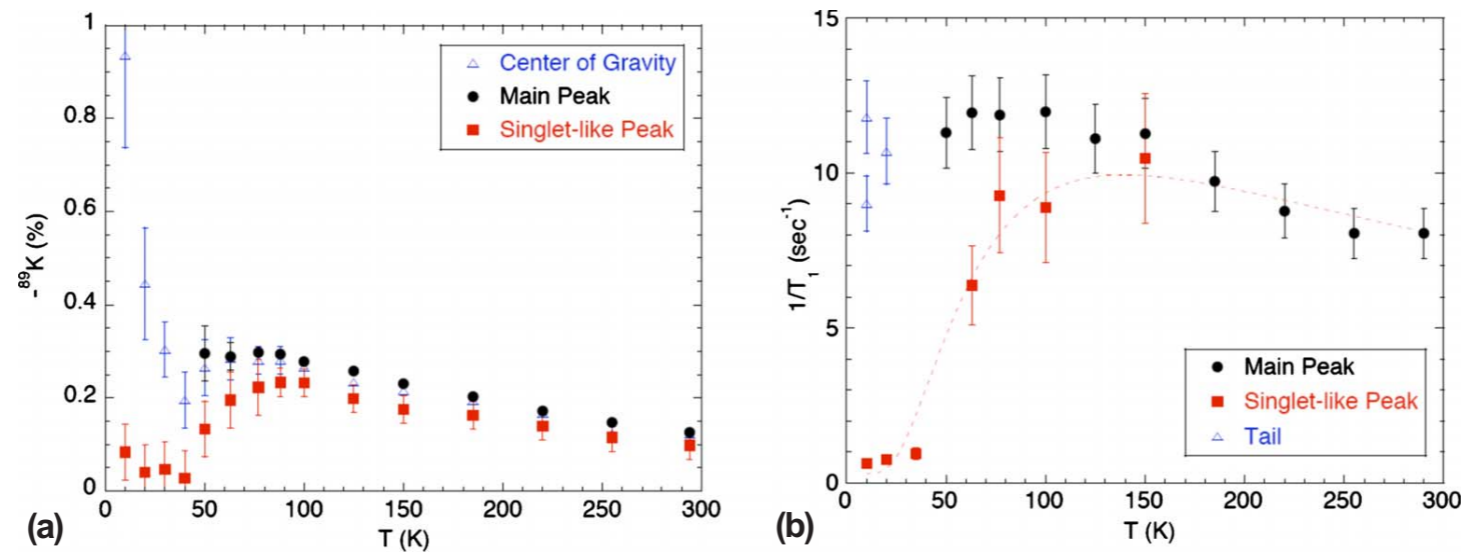


FIG. 15. (Color online) Temperature dependence of the paramagnetic Knight shift, $-^{89}\text{K}$ (a) and the relaxation rate, $1/T_1$ (b) for the “main” (lower frequency) peak and the singletlike (higher frequency) peak of Fig. 14(b). The dotted line is an empirical fit $1/T_1 \sim C/T \exp(-\Delta/k_B T)$ with $\Delta/k_B \sim 140$ K. Integrated intensities of the two are roughly equal.

Triplet and in-gap magnetic states in the ground state of the quantum frustrated fcc antiferromagnet Ba_2YMoO_6

J. P. Carlo,^{1,2,*} J. P. Clancy,¹ T. Aharen,³ Z. Yamani,² J. P. C. Ruff,¹ J. J. Wagman,¹ G. J. Van Gastel,¹ H. M. L. Noad,¹ G. E. Granroth,⁴ J. E. Greedan,^{3,5} H. A. Dabkowska,⁵ and B. D. Gaulin^{1,5,6}

¹*Department of Physics and Astronomy, McMaster University, Hamilton, Ontario L8S 4M1, Canada*

²*Canadian Neutron Beam Centre, National Research Council, Chalk River, Ontario K0J 1J0, Canada*

³*Department of Chemistry, McMaster University, Hamilton, Ontario L8S 4M1, Canada*

⁴*Neutron Scattering Sciences Division, Oak Ridge National Laboratory, Oak Ridge, TN, USA*

⁵*Brockhouse Institute for Materials Research, McMaster University, Hamilton, Ontario L8S 4M1, Canada*

⁶*Canadian Institute for Advanced Research, Toronto, Ontario M5G 1Z8, Canada*

(Received 20 May 2011; revised manuscript received 16 August 2011; published 19 September 2011)

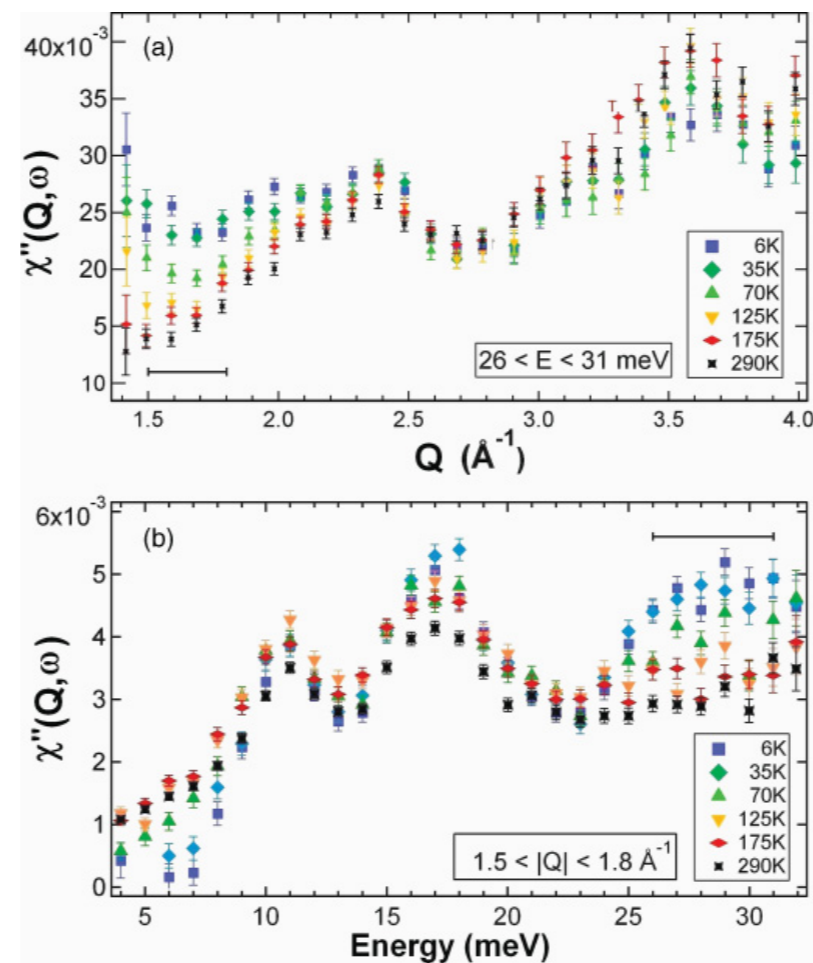
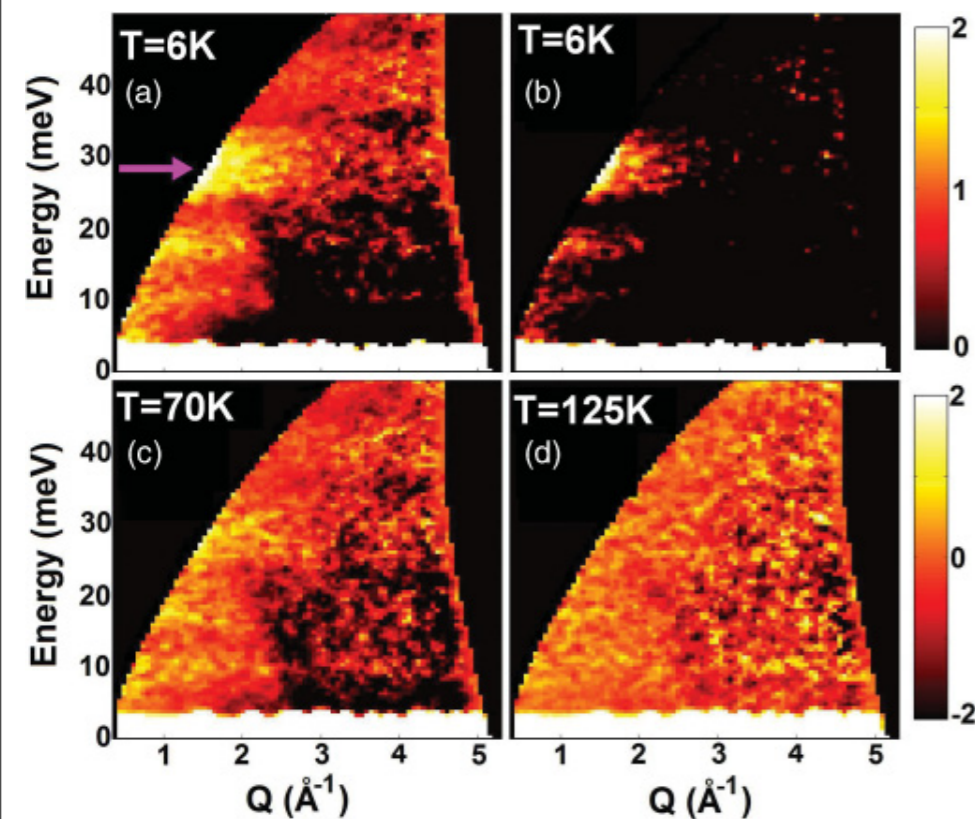


FIG. 3. (Color online) (a) $\chi''(Q, \hbar\omega)$ plotted versus Q for six temperatures, integrated in energy between 26 and 31 meV. (b) $\chi''(Q, \hbar\omega)$ plotted versus energy for six temperatures, integrated in Q over the range $1.5 \text{ \AA}^{-1} < Q < 1.8 \text{ \AA}^{-1}$. The scattering centered on ~ 28 meV exists only at low $Q < 2.5 \text{ \AA}^{-1}$ and at low $T < 125$ K, and is therefore magnetic in origin and consistent with a weakly dispersive spin-triplet excitation.

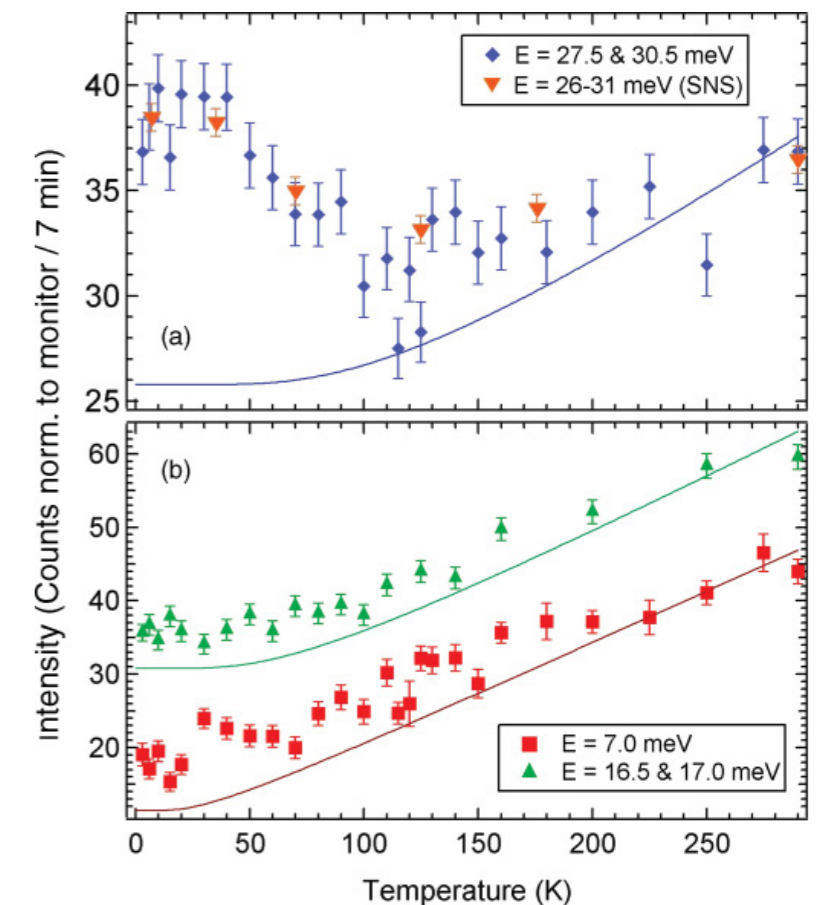


FIG. 4. (Color online) (a) Temperature dependence of the background-subtracted scattering intensity at $Q = 1.7 \text{ \AA}^{-1}$ at the average of 27.5 and 30.5 meV, collected with the C5 triple-axis spectrometer, showing a characteristic fall-off of the triplet intensity toward zero at ~ 125 K; normalized SEQUOIA (SNS) data at 26–31 meV is included for reference. (b) Temperature dependence of the background-subtracted intensity at 7 meV and a 16.5–17 meV energy transfer. The solid lines represent fits of the $T > 200$ K data to the thermal occupancy factor. Excess low-temperature scattering is attributed to either (a) the triplet excitation, or (b) magnetic states within the gap.

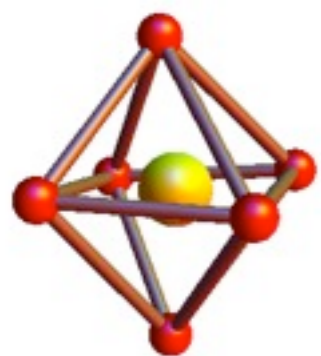
FIG. 2. (Color online) (a), (c), (d) Dynamic susceptibility $\Delta\chi''(Q, \hbar\omega)$ at $T = 6, 70,$ and 125 K, where $\chi''(Q, \hbar\omega)$ at $T = 175$ K has been subtracted from each to isolate the magnetic scattering, as described in the text. (b) shows $\Delta\chi''(Q, \hbar\omega)$ at $T = 6$ K with $T = 175$ K subtracted, but with the plotted intensity scale range restricted to >0 only, thus highlighting where $\chi''(Q, \hbar\omega)$ at 6 K exceeds that at 175 K. The lower intensity scale refers to (a), (c), and (d), and the upper refers to (b).

Periodic Table of the Elements

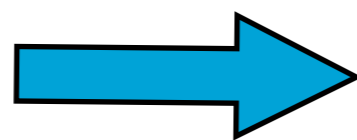
| | | | | | | | | | | | | | | | | | | | | | | | | | | | | | | | | | | | | | | | | |
|---|----|----|----|----|-----|----|-----|-----|----|-----|----|-----|----|-----|----|-----|----|-----|----|-----|-----|-----|-----|-----|-----|-----|-----|-----|-----|-----|-----|-----|-----|-----|-----|-----|-----|-----|-----|-----|
| 1 | IA | 1 | H | 2 | IIA | 2 | He | 0 | | | | | | | | | | | | | | | | | | | | | | | | | | | | | | | | |
| 2 | | 3 | Li | 4 | Be | 5 | B | 6 | C | 7 | N | 8 | O | 9 | F | 10 | Ne | | | | | | | | | | | | | | | | | | | | | | | |
| 3 | | 11 | Na | 12 | Mg | 13 | Al | 14 | Si | 15 | P | 16 | S | 17 | Cl | 18 | Ar | | | | | | | | | | | | | | | | | | | | | | | |
| 4 | | 19 | K | 20 | Ca | 21 | Sc | 22 | Ti | 23 | V | 24 | Cr | 25 | Mn | 26 | Fe | 27 | Co | 28 | Ni | 29 | Cu | 30 | Zn | 31 | Ga | 32 | Ge | 33 | As | 34 | Se | 35 | Br | 36 | Kr | | | |
| 5 | | 37 | Rb | 38 | Sr | 39 | Y | 40 | Zr | 41 | Nb | 42 | Mo | 43 | Tc | 44 | Ru | 45 | Rh | 46 | Pd | 47 | Ag | 48 | Cd | 49 | In | 50 | Sn | 51 | Sb | 52 | Te | 53 | I | 54 | Xe | | | |
| 6 | | 55 | Cs | 56 | Ba | 57 | *La | 72 | Hf | 73 | Ta | 74 | W | 75 | Re | 76 | Os | 77 | Ir | 78 | Pt | 79 | Au | 80 | Hg | 81 | Tl | 82 | Pb | 83 | Bi | 84 | Po | 85 | At | 86 | Rn | | | |
| 7 | | 87 | Fr | 88 | Ra | 89 | +Ac | 104 | Rf | 105 | Ha | 106 | Sg | 107 | Ns | 108 | Hs | 109 | Mt | 110 | 111 | 112 | 113 | 114 | 115 | 116 | 117 | 118 | 119 | 120 | 121 | 122 | 123 | 124 | 125 | 126 | 127 | 128 | 129 | 130 |

| | | | | | | | | | | | | | | |
|---------------------|----|----|----|----|----|----|----|----|----|----|-----|-----|-----|-----|
| * Lanthanide Series | 58 | 59 | 60 | 61 | 62 | 63 | 64 | 65 | 66 | 67 | 68 | 69 | 70 | 71 |
| | Ce | Pr | Nd | Pm | Sm | Eu | Gd | Tb | Dy | Ho | Er | Tm | Yb | Lu |
| + Actinide Series | 90 | 91 | 92 | 93 | 94 | 95 | 96 | 97 | 98 | 99 | 100 | 101 | 102 | 103 |
| | Th | Pa | U | Np | Pu | Am | Cm | Bk | Cf | Es | Fm | Md | No | Lr |

$Re^{6+}, Os^{7+}, Mo^{5+}$



xy, xz, yz



SOC



$J=1/2$

$J=3/2$

$$M = \mathcal{P}_{\frac{3}{2}} [2S + (-l)] \mathcal{P}_{\frac{3}{2}} = 0!!$$

$$M \sim 0.6 - 0.7 \mu_B$$

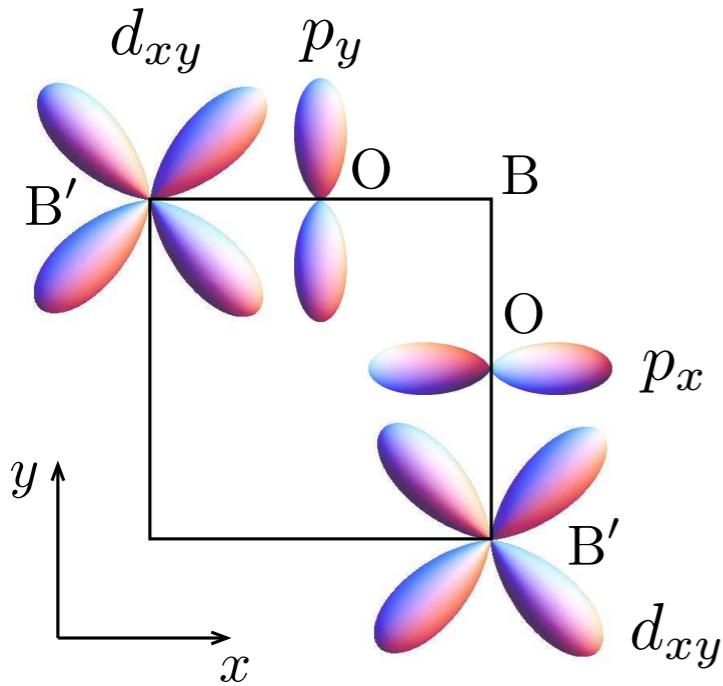
$$\lambda \sim 1481 K \text{ in } Mo^{5+}$$

$$M \sim 1.3 - 1.4 \mu_B$$

for Ba_2YMoO_6

for $Ba_2CaReO_6, Ba_2LiOsO_6, Ba_2CaOsO_6$

Exchange interaction and singlets



$$H_{XY} = J \left(\mathbf{S}_{i,xy} \cdot \mathbf{S}_{j,xy} - \gamma n_{i,xy} n_{j,xy} \right) - \lambda \mathbf{l}_i \cdot \mathbf{S}_i - \lambda \mathbf{l}_j \cdot \mathbf{S}_j$$

$$\mathbf{S}_{i,xy} \equiv \mathbf{S}_i n_{i,xy}$$

Singlets

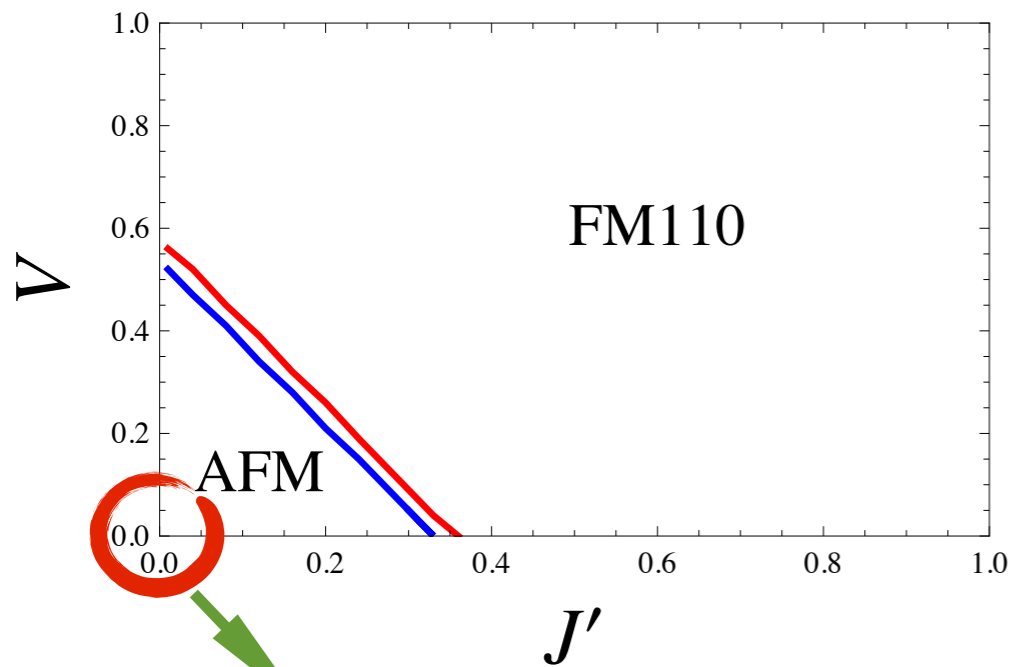
$$J \gg \lambda \quad \frac{1}{\sqrt{2}} \left(|S_i^z = \frac{1}{2}, xy\rangle |S_j^z = -\frac{1}{2}, xy\rangle - |S_i^z = -\frac{1}{2}, xy\rangle |S_j^z = \frac{1}{2}, xy\rangle \right)$$

$$J \ll \lambda \quad \frac{1}{\sqrt{2}} \left(|j^z = \frac{1}{2}\rangle_i |j^z = -\frac{1}{2}\rangle_j - |j^z = -\frac{1}{2}\rangle_i |j^z = \frac{1}{2}\rangle_j \right)$$

$J \ll \lambda$

Projecting to $j=3/2$ basis

$$\left\{ \begin{array}{l} \tilde{S}_{i,xy}^x = \frac{j_i^x}{4} - \frac{j_i^z j_i^x j_i^z}{3} \\ \tilde{S}_{i,xy}^y = \frac{j_i^y}{4} - \frac{j_i^z j_i^y j_i^z}{3} \\ \tilde{S}_{i,xy}^z = \frac{3j_i^z}{4} - \frac{j_i^z j_i^z j_i^z}{3} \\ \tilde{n}_{i,xy} = \frac{3}{4} - \frac{(j_i^z)^2}{3} \end{array} \right.$$



Large quantum fluctuation

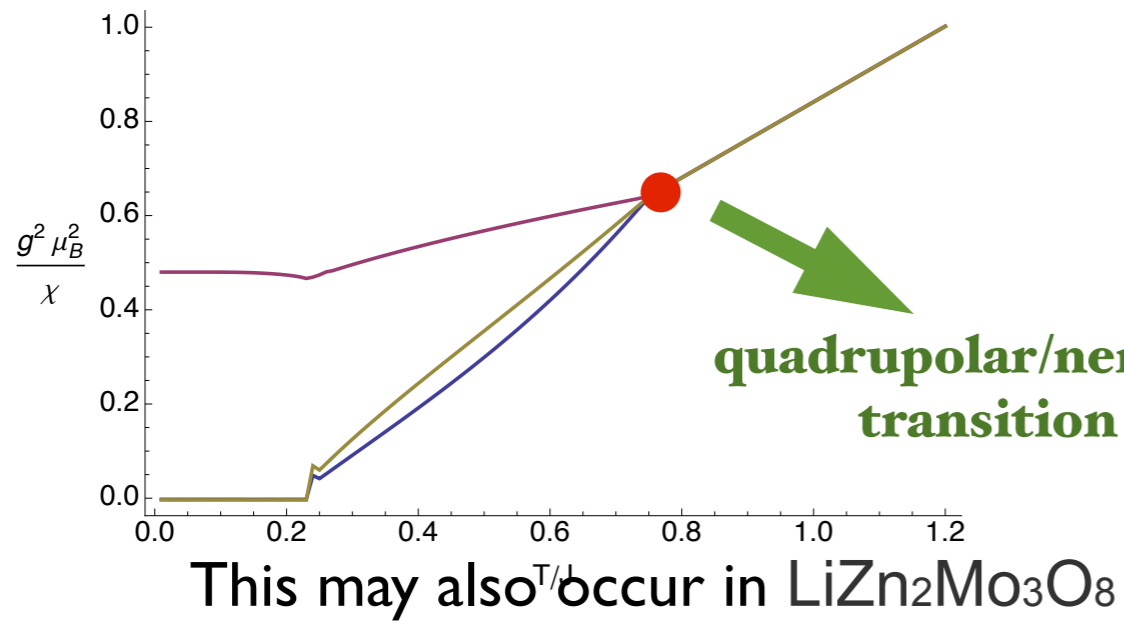


FIG. 12. (Color online) Inverse susceptibility for for $J' = 0.2$, $V = 0.3$. Blue (lower) curve: $1/\chi_{xx}$, red (upper) curve: $1/\chi_{zz}$, yellow (middle) curve: $1/\chi_{\text{powder}}$. For these parameters the quadrupolar transition is at $T/J \approx 0.75$, and the ferromagnetic transition is at $T/J \approx 0.23$.

Two Curie regimes!

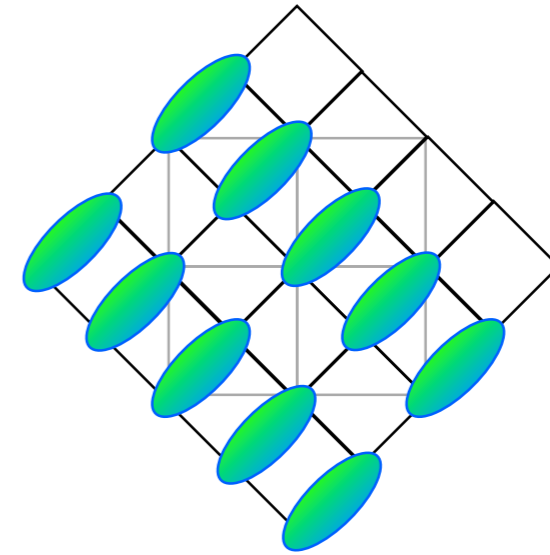


FIG. 16. Columnar dimer state within an XY plane. The gray square indicates the face of a conventional cubic unit cell, while the black lines connect the FCC nearest neighbors within the plane, which form a 45° rotated square lattice.

If one restricts to dimer configuration, the hamiltonian can be mapped to a quantum-dimer model on an FCC lattice.

Coupling between the layers lifts the degeneracy of the VBS states.

GS can also be some irregular VBS so that the distortion due to dimers is reduced.